International Journal of Hydrogen Energy 66 (2024) 33–39

Contents lists available at ScienceDirect

International Journal of Hydrogen Energy

journal homepage: www.elsevier.com/locate/he

# Metal-decorated boron phosphide (BP) biphenylene and graphenylene networks for ultrahigh hydrogen storage

Ikram Djebablia [c,d], Yusuf Zuntu Abdullahi [a,b,*], Kamel Zanat [d], Fatih Ersan [a]

[a] Department of Physics, Aydin Adnan Menderes University, Aydin 09010, Turkey
[b] Department of Physics, Faculty of Science, Kaduna State University, P.M.B. 2339 Kaduna State, Nigeria
[c] Radiation and Matter Physics Laboratory, Matter Sciences Department, Mohamed-Cherif Messaadia University, P.O. Box 1553, Souk-Ahras, 41000, Algeria
[d] Physics laboratory at Guelma, Faculty of Mathematics, Computing and Material Sciences, University 8 May 1945 Guelma, P.O. Box 401, Guelma 24000, Algeria

ARTICLE INFO

*Keywords:*
Hydrogen storage
Density functional theory
Alkali metal decorated boron phosphide biphenylene and graphenylene systems
Adsorption properties

ABSTRACT

The synthesized carbon-based biphenylene materials have contributed to the recent increase in interest in inorganic biphenylene counterpart. It is expected that the inorganic biphenylene material will have suitable functionalities for different energy harvesting applications. In this study, we conducted first-principles density functional theory (DFT) calculations and thermodynamic analysis to explore the hydrogen ($H_2$) storage properties of pristine BP-biphenylene (b-BP) and BP-graphenylene (g-BP) monolayers and alkali metals (AM=Li, Na, K) decorated b-BP (labeled as b-BP(AM)) and g-BP (labeled as g-BP(AM)) systems. Both b-BP and g-BP monolayers exhibit a weak affinity for ($H_2$) molecules. However, b-BP(AM) and g-BP(AM) overcome this limitation and exhibit the ability to adsorb multiple $H_2$ molecules. The positive charge generated by the AM adatoms is the cause of the neighboring $H_2$ molecules becoming polarized due to electron transfer to the b-BP and g-BP monolayers. This polarization facilitates their binding through van der Waals interactions, making the surrounding suitable to accommodate a significant amount of $H_2$ molecules. The storage capacities for b-BP(Li) and g-BP(Li) systems are 9.05 wt% and 6.99 wt% respectively, when operating under practical conditions. Notably, these values exceed the US Department of Energy's target of 5.50 wt% by 2025 and highlight the potential of b-BP(AM) and g-BP(AM) systems as promising materials for hydrogen storage applications.

## 1. Introduction

The widespread utilization of fossil fuels as the predominant energy source has resulted in serious issues like global warming and environmental pollution. It is imperative to address these issues by developing sustainable, affordable and environmentally friendly energy sources and storage technologies. Hydrogen is a suitable energy carrier because of its high energy density, renewable nature, abundance, and cleanliness, and it is widely recognized as having outstanding potential for energy applications [1]. However, the major obstacle to transitioning to a renewable energy economy based on synthetic hydrogen fuel is the storage problem [2]. Therefore, the development of novel materials that can store hydrogen at acceptable rates, have become pivotal aspects of contemporary scientific discourse [3–6]. This urgency arises because conventional methods such as pressurized tanks and cryogenic liquid hydrogen fail to meet the necessary standards for vehicle applications, primarily due to issues related to safety concerns and low volumetric density [1,7]. In general, materials that are desirable for on-board hydrogen storage are expected to meet the technical criteria set by the US Department of Energy (DOE). These criteria include high gravimetric density, quick kinetics, low toxicity, moderate working temperature, great reversibility, and/or low cost.

Research efforts to identify materials that satisfied the aforementioned criteria have resulted in the development of new porous monolayer [8–16] and related materials [17–26]. Among them, the newly synthesized carbon-based biphenylene materials [27] have opened up new possibilities for hydrogen storage due to their numerous related functionalities. However, like other pristine adsorbents porous materials, the practical utility of these nanostructures for hydrogen storage is hindered by the relatively weak Van der Waals (vdW) interaction between adsorbed ($H_2$) molecules and host surfaces under typical temperature and pressure conditions [28–30]. Thus, it is necessary to enhance the binding energy values between hydrogen molecules ($H_2$) and the host materials.

To achieve enhance hydrogen adsorption rate, various strategies such as mechanical strain, cation/anion substitution, nanoscaling, defect engineering and metal functionalization have been used to modify the performance of host materials [31–35]. Metal functionalization has

* Corresponding author at: Department of Physics, Aydin Adnan Menderes University, Aydin 09010, Turkey.
*E-mail addresses:* yzabdullahi.edu.tr@adu.edu.tr (Y.Z. Abdullahi), fatih.ersan@adu.edu.tr (F. Ersan).

https://doi.org/10.1016/j.ijhydene.2024.04.080
Received 6 February 2024; Received in revised form 28 March 2024; Accepted 5 April 2024

proven to be an effective technique for enhancing hydrogen storage capacity and overcoming the dilemma between reversibility and the desorption temperature of intrinsic 2D materials [29,30,36–38]. For instance, previous theoretical studies have shown that monolayers decorated with alkali metals (AM = Li, Na, K) adatoms are advantageous for boosting $H_2$ adsorptionenergy [36,38–47]. Denis et al. reported the hydrogen storage capabilities of Li-decorated biphenylene sheets, they found a hydrogen gravimetric density of 7.4% wt, accompanied by an average adsorption energy of 0.20 eV/$H_2$ [39]. Following this trend, Mane et al. explored the Zr-doped biphenylene and reported a storage capacity of 9.95 weight wt%, with an average hydrogen adsorption energy of 0.4 eV/$H_2$ [40]. In separate study, Mahamiya, et al. tested the hydrogen storage ability of K and Ca modified biphenylene sheets, they predicted that each K and Ca adatom could adsorb 5$H_2$ molecules, following with 11.90 and 11.63 weight percent of $H_2$, respectively [41]. Kaewmaraya, et al. have found 6.76 wt% and 6.66 wt% of hydrogen uptake for divacancy biphenylene functionalized by Li and Na [36]. Additionally Hussain et al. have investigated hydrogen storage properties of graphenylene monolayer decorated with light metals, they found that each dopant can adsorb multiple $H_2$ molecules leading to 6.14 wt% hydrogen capacity [38].

In this study, for the first time we carried out first-principles calculations based on density functional theory (DFT) [48] to study the hydrogen storage properties of pristine BP-biphenylene (b-BP) and BP-graphenylene (g-BP) and AM decorated b-BP and g-BP systems. Henceforth, we shall level AM decorated b-BP as b-BP(AM) while AM decorated g-BP as g-BP(AM) systems. The findings reveal that pristine b-BP and g-BP monolayers are inefficient for $H_2$ storage. However, the $H_2$ adsorption energy improved for b-BP(AM) and g-BP(AM) systems. b-BP(AM) can adsorb a total of 32$H_2$ molecules with an average adsorption energies of −0.18, −0.16, and −0.14 eV/$H_2$ for b-BP(Li), b-BP(Na), and b-BP(K) systems respectively. For the g-BP(AM) cases, we found a total of 48 $H_2$ molecules with an average adsorption energies of −0.20, −0.17, and −0.15 eV/$H_2$ for g-BP(Li), g-BP(Na), and g-BP(K) systems, respectively. Furthermore, the b-BP(Li) and g-BP(Li) systems attain the storage capacities of 9.05 wt% and 6.99 wt% at the practical temperature and pressure, respectively, exceeding the US Department of Energy's target value of 5.50 wt% by 2025. Therefore, b-BP(AM) and g-BP(AM) systems clearly shows a very prospect for hydrogen storage applications.

## 2. Computational details

All current calculations were achieved by DFT [48] calculations using the Vienna Ab initio Simulation Package (VASP) [49]. The interaction between the valence and core electrons is described on the basis of the projected augmented wave (PAW) method [50]. The electron exchange–correlation effects is expressed by the generalized gradient approximation (GGA) method with Perdew–Burke–Ernzerhof (PBE) functional [50]. Moreover, vdW corrections were considered by using DFT-D2 method of Grimme throughout the calculations [51]. The cutoff energy was set to 500 eV, and the Brillouin zone was sampled using Monkhorst–Pack method with automatically generated (3 × 3 × 1) k-point mesh [52]. The convergence criteria of energy and atomic force were set to $10^{-6}$ and $10^{-5}$ eV Å$^{-1}$ in the geometric optimization and static calculations. To avoid the interactions between adjacent layers, a vacuum thickness of at most 17 Å along the z direction was included for all monolayers, respectively. As for the calculation of isolated $H_2$ molecule, it was packed into a 15 Å periodic edge cubic box. Ab initio molecular dynamics (AIMD) simulations was performed within the framework of the NVT-ensemble to check the stability of host materials at 300 K with a time-step set of 1 fs for a total time scale of 5 ps [53]. Charge transfer mechanism was studied by employing Bader analysis [54]. The stability of b-BP(AM) and g-BP(AM) systems is calculated by the adsorption energy ($E_{ads}$) relation expressed as

$$E_{ads} = \frac{E_{b-BP(AM)(g-BP(AM))} - E_{b-BP(g-BP)} - nE_{AM}}{n} \quad (1)$$

where $E_{b-BP(AM)(b-BP(AM))}$, $E_{b-BP(g-BP)}$ and $nE_{AM}$ stand for the total energies of b-BP(AM)(b-BP(AM)), pristine b-BP(g-BP) and isolated AM atoms, respectively. However $n$ represent the total number of AM adatoms.

The adsorption energy ($E_{ads}$) of $H_2$ molecules on b-BP(AM) and g-BP(AM) systems is calculated as,

$$E_{ads} = \frac{E_{(b-BP(AM)@mH_2)(g-BP(AM)@mH_2)} - E_{b-BP(AM)(g-BP(AM))} - mE_{H_2}}{m} \quad (2)$$

where, $E_{(b-BP(AM)@mH_2)(g-BP(AM)@mH_2)}$, $E_{H_2}$ and $m$ terms represent the total energy values of b-BP(AM)(g-BP(AM)) with adsorbed $mH_2$ molecules, isolated $H_2$ molecule and the number of $H_2$ molecules adsorbed on b-BP(AM)(g-BP(AM)) systems, respectively. The gravimetric hydrogen capacity (wt%) was calculated using the following expression:

$$H_2\ (wt\%) = \frac{MH_2}{(MH_2 + M_{host})} * 100 \quad (3)$$

here, $MH_2$ and $M_{host}$ represent the mass of the total stored $H_2$ molecules and the mass of b-BP(AM)(g-BP(AM)) systems, respectively.

The adsorption–desorption properties of $H_2$ molecules under operating conditions (temperature and pressure) were further investigated by thermodynamic analysis using the grand canonical partition function (z).

$$Z = 1 + \sum_{i=1}^{n} \frac{\exp E_i^{ads} - \mu}{K_B T} \quad (4)$$

where, $n$ is the maximum number of adsorbed hydrogen ($H_2$) molecules. while, $E_i^{ads}$, $\mu$, $K_B$, and $T$ are the adsorption energy of the $i$th adsorbed $H_2$ molecule, chemical potential of the gas phase of the $H_2$ molecule, the Boltzmann constant (1.38 × $10^{-23}$ J/K), and temperature, respectively. The previous reports provide the details of the calculations [29, 36]. It is worth noting that the pressure and temperature that work best for adsorption (desorption) of $H_2$ are 30 (3) atm and 25 (100) °C, respectively.

## 3. Results and discussion

### 3.1. Hydrogen adsorption on pristine b-BP and g-BP monolayers

Fig. 1 shows the optimized (2 × 2 × 1) b-BP and g-BP supercell. There are the same number of B and P atoms in each structure. Consistent with the carbon-based biphenylene structure, the b-BP structure features an octagonal cavity formed by hexagonal $B_3P_3$ rings. These hexagonal $B_3P_3$ rings are connected next to each other via the B-P bond. The g-BP structure is similar to the b-BP but has a dodecagonal cavity. In each b-BP and g-BP structure, both B and P atoms contribute equally to the cavity, with no dangling bonds. The optimized lattice constants of (2 × 2 × 1) b-BP and g-BP supercell were estimated to be $a$ = 11.80 Å, $b$ = 9.75 Å and $a = b$ = 17.61 Å, respectively. It is noted that the b-BP monolayer is anisotropic along the $a/b$ lattice direction because of its rectangular symmetry, while that for g-BP monolayer with hexagonal symmetry is isotropic ($a = b$).

Next, we introduced the $H_2$ molecule at a certain height above the b-BP and g-BP surfaces. Eight different adsorption sites on the b-BP and g-BP surfaces were considered for perpendicular and parallel $H_2$ orientations. These adsorption sites are located at the top of the octagonal/decagonal cavity ($S_1$), the square ($S_2$) and hexagonal ($S_3$) rings, the bridging sites ($S_4$, $S_5$ and $S_6$), and the boron ($T_B$) and phosphorus ($T_P$) atoms (see Fig. 1). Firstly, we performed with spin-polarized optimization calculations for all structures and found non-magnetic properties. For later convenience, b-BP and g-BP with adsorbed $H_2$ molecule are referred to as b-BP@$H_2$ and g-BP@$H_2$, respectively. On the other hand, b-BP(AM) and g-BP(AM) with adsorbed $H_2$ molecule are classified as b-BP(AM)@$H_2$ and g-BP(AM)@$H_2$, respectively. The

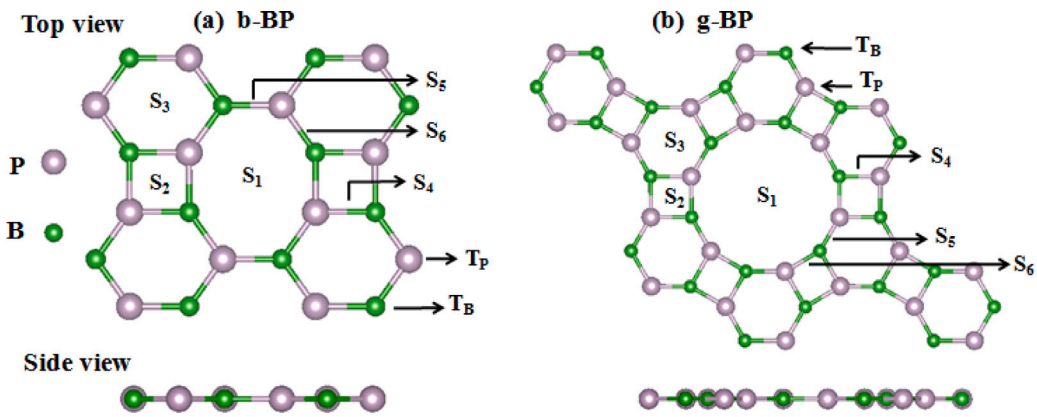


**Fig. 1.** Top and side view of the optimized (2 × 2) supercell: (a) b-BP and (b) g-BP with the possible adsorption sites ($S_1$, $S_2$, $S_3$, $S_4$, $S_5$, $S_6$, $T_B$, $T_P$).

corresponding $H_2$ adsorption energy ($E_{ads}$) values for b-BP(AM)@$H_2$ and g-BP(AM)@$H_2$ systems are shown in Fig. S1. The preferred adsorption sites for perpendicularly aligned $H_2$ are the $S_4$ and $S_2$ sites of the b-BP and g-BP surfaces, respectively. The estimated $E_{ads}$ values for b-BP@$H_2$ and g-BP@$H_2$ systems are −0.07 eV and −0.03 eV, respectively. These low $E_{ads}$ values severely hamper their practical performance in $H_2$ storage applications.

### 3.2. Alkali metals (AM = Li, Na, K) decorated b-BP and g-BP monolayers

As mentioned above, the pristine b-BP and g-BP monolayers are thermodynamically unfavorable for $H_2$ molecule adsorption, however, previous reports [36,38,41] confirmed that the $H_2$, $E_{ads}$ value can be improved for AM-decorated surfaces. Therefore, AM adatoms are introduced on the b-BP and g-BP surfaces to improve the $H_2$ $E_{ads}$ values. First, we identified the favorable adsorption site for a single AM adatom adsorbed b-BP and g-BP surfaces, as shown in Fig. S2. The preferred adsorption sites are $S_3$, $S_1$ and $S_1$ for b-BP(Li), b-BP(Na) and b-BP(K) with $E_{ads}$ values of −2.28 eV, −1.76 eV and −2.14 eV. The estimated adatom height ($h$) values above the surfaces are 1.5, 1.6, and 2.12 Å for b-BP(Li), b-BP(Na), and b-BP(K) systems, respectively. On the other hand, the preferred adsorption site for g-BP(Li), g-BP(Na) and g-BP(K) system is the $S_2$ site with $E_{ads}$ values of −2.29 eV, 1.69 eV and 2.08 eV, respectively. Their corresponding $h$ values are 1.62, 2.21, and 2.61 Å for g-BP(Li), g-BP(Na), and g-BP(K), respectively. Our estimated $E_{ads}$ values show that AM adatoms bind strongly to the b-BP and g-BP surfaces (see Table 1).

It should be noted that both the b-BP and g-BP systems have the lowest $h$ values and, accordingly, the highest $E_{ads}$ values. The differences in the $E_{ads}$ values for b-BP(AM) and g-BP(AM) systems are largely determined by the electron transfer between the AM adatoms and the b-BP and g-BP monolayers. Bader charge analysis shows that the AM adatoms transfer electrons to the b-BP and g-BP monolayers. The calculated values are 0.88, 0.87, 0.86 $e^-$ for b-BP(Li), b-BP(Na), b-BP(K) while those for g-BP(Li), g-BP(Na), and g-BP(K) systems are 0.88, 0.88, and 0.87 $e^-$ respectively. The values show that the larger the charge transfer, the closer the AM adatoms are to the b-BP and g-BP surfaces. Consequently, there is increased polarization between the AM adatoms and the b-BP and g-BP monolayers (see Table 1).

Following the investigation of single AM adatoms on b-BP and g-BP, we proceed to study the full-coverage AM adatoms on both sides of b-BP and g-BP monolayers. As displayed in Fig. 2, no reconstruction was observed on both the b-BP and g-BP surfaces after full structural relaxation. Moreover, the b-BP and g-BP surfaces do not have any clustering tendencies for AM atoms. It was found that the b-BP monolayer can accommodate at most eight AM adatoms. While the g-BP monolayer can accommodate 16 AM adatoms. Table S1 present the calculated $E_b$ values, stable sites and the $h$ values for b-BP(AM) and g-BP(AM) systems, respectively. The estimated values for b-BP(AM) and g-BP(AM) with full coverage AM adatoms follow the same pattern as that described above for b-BP(AM) and g-BP(AM) single AM adatoms. It should be noted that the ionic bonding exists between the AM adatoms and the b-BP and g-BP systems. The ionic bonding nature of AM adatoms on b-BP and g-BP surfaces was elucidated using the electron localization function (ELF). Fig. S3 shows the ELF plots with ranges of isosurface values indicating the presence of a localized charge. This charge accumulations makes b-BP(AM) and g-BP(AM) suitable for adsorbing $H_2$ molecules. We also projected density of states (PDOS) of b-BP(8 AM) and g-BP(16 AM) systems to reveal their atomic orbital contributions in the vicinity of Fermi level (See Fig. 3). The PDOS plots show that all b-BP(8 AM) and g-BP(16 AM) systems exhibit metallic property (see Fig. S4).

**Table 1**
The calculated $E_{ads}$, $h$ and charge transfer (Q) for b-BP(AM) and g-BP(AM) systems. $h$ is defined as the difference in the z-coordinate of the AM adatoms and the average of the z-coordinate of all the B/P atoms in the b-BP and g-BP systems.

| System | Stable site | $E_{ads}$ (eV/atom) | $h$ (Å) | Q ($e^-$) |
|---|---|---|---|---|
| b-BP(8Li) | $S_3$ | −1.97 | 1.68 | 0.86 |
| b-BP(8Na) | $S_1$ | −1.35 | 1.77 | 0.80 |
| b-BP(8K) | $S_1$ | −1.47 | 2.30 | 0.68 |
| g-BP(16Li) | $S_2$ | −2.01 | 1.78 | 0.76 |
| g-BP(16Na) | $S_2$ | −1.30 | 1.78 | 0.86 |
| g-BP(16K) | $S_2$ | −1.46 | 1.78 | 0.70 |

AIMD simulations were performed on b-BP(AM) and g-BP(AM) systems at T = 300 K for 5 ps to ascertain their thermal stability. No geometry constraints are imposed on the b-BP(8 AM) and g-BP(16 AM) systems during MD calculations. Fig. S5 demonstrates the snapshots of the top and side view of these structures as an inset. The b-BP(8 AM) and g-BP(16 AM) structures have minor buckling, but there is no evidence of structural reconstruction. Moreover, there is minimal fluctuation in the variation of total energy vs time for all systems. It is clear that these b-BP(8 AM) and g-BP(16 AM) materials at 300 K are ideal for $H_2$ storage application.

### 3.3. Hydrogen storage on b-BP(AM) and g-BP(AM) systems

Having established the stable b-BP(8 AM) and g-BP(16 AM) systems, we evaluate the $H_2$ adsorption properties on these structures. The first step is to optimize a single $H_2$ molecule in each systems to determine the $E_{ads}$ values. All atoms in both the b-BP (8 AM)@$H_2$ and g-BP (16 AM)@$H_2$ systems can move freely during optimization without any structural constraints. Our estimated $E_{ads}$ values for b-BP(8 AM)@$H_2$ and g-BP(16 AM)@$H_2$ suggest an improvement compared to those

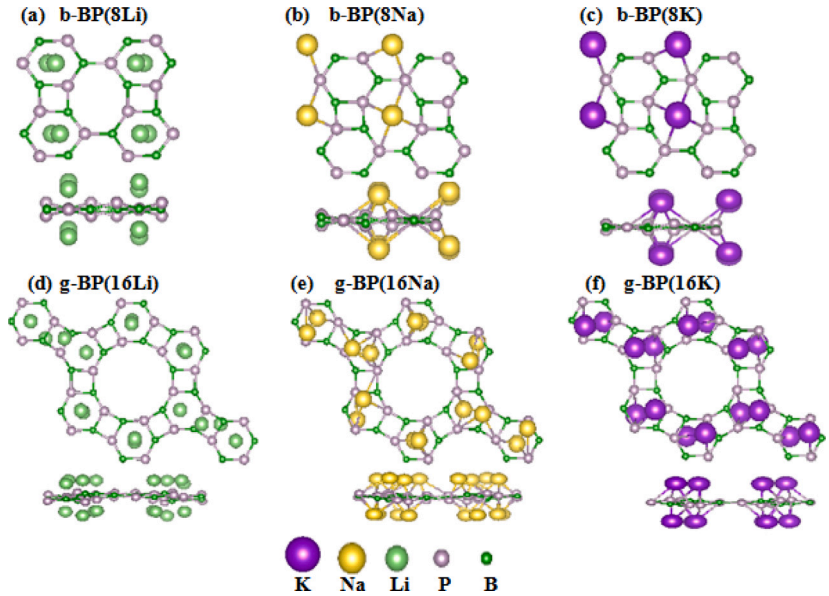


**Fig. 2.** Optimized structures of b-BP(8 AM) and g-BP(16 AM) systems (Top and side views).

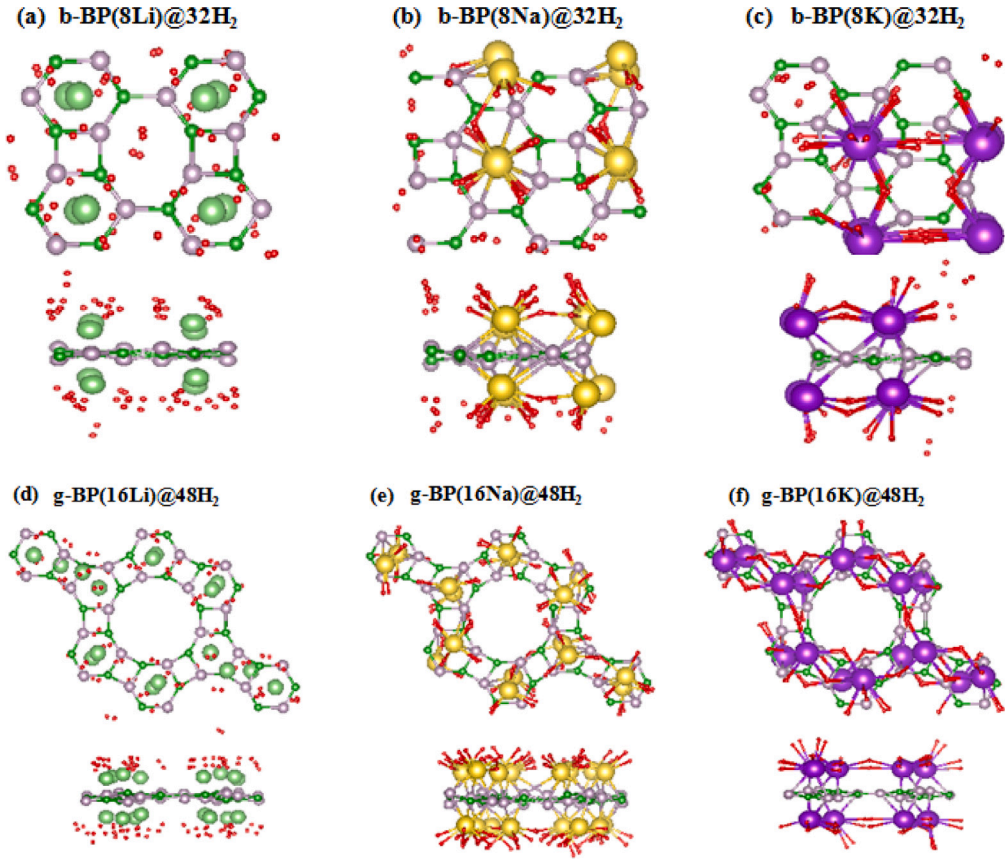


**Fig. 3.** Optimized b-BP(8 AM)@$32H_2$ and g-BP(16 AM)@$48H_2$ structures.

obtained from the b-BP@$H_2$ and g-BP@$H_2$ systems. The estimated $E_{ads}$ values are summarized in Table 2. We then performed a series of optimization calculations by increasing the number of $H_2$ molecules until a maximum of $32H_2$ ($16H_2$ on top and $16H_2$ on down) molecules and $48H_2$ ($24H_2$ on top and $H_2$ on down) molecules were accommodated on the b-BP(8 AM) and g-BP(16 AM) surfaces, respectively (see Fig. 4).

The estimated $E_{ads}$ values are −0.20, −0.18 and −0.14 eV/$H_2$ for b-BP(8Li) @$32H_2$, b-BP(8Na)@$32H_2$, and b-BP(8K)@$32H_2$ systems with storage capacities of 10.38, 8.60 and 7.34 w%, respectively. On the

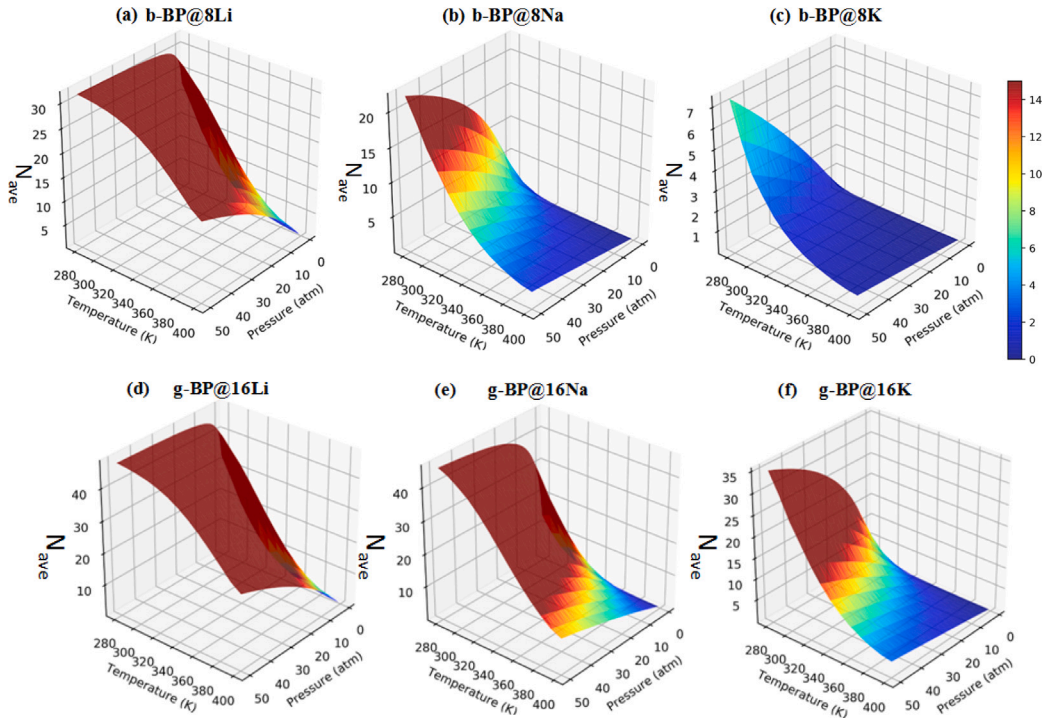


**Fig. 4.** The averaged number of $H_2$ molecules (Nave) adsorbed on (a) b-BP(8Li), (b) b-BP(8Na), (c) b-BP(8K), (d) g-BP(16Li), (e) g-BP(16Na), and (f) g-BP(16K) as a function of practical temperatures and pressures.

other hand, the $E_{ads}$ values are −0.20, −0.17 and −0.15 eV/$H_2$ for g-BP(16Li)@48$H_2$, g-BP(16Na)@48$H_2$, and g-BP(16K)@48$H_2$ systems with storage capacities of 7.99, 6.59 and 5.61 wt%, respectively. The obtained maximum wt% values at 0 K are either comparable with or larger than the previously reported values for similar inorganic monolayer materials e.g SiC (8.27) [55] and boron hydride (11.70) [56]. Table 2 list all $E_{ads}$ values for all b-BP(AM)@$H_2$ and g-BP(AM)@$H_2$ systems. We also provided the gravimetric density (wt%), H–H bond distance ($d_{(H–H)}$), and the lowest Hydrogen height ($h$) values above the b-BP and g-BP surfaces. It is obvious that the $E_{ads}$ values are negative, which implies that $H_2$ would preferentially be physisorbed on the b-BP(AM) and g-BP(AM) surfaces. However, the $E_{ads}$ values are disparate for each system and gradually decrease in the order of the Li, Na, and K adatoms. This is mainly due to their difference in electronegativity. We verified this assertion by examining the electron transfer between the charged AM ions and the surrounding $H_2$ molecules. Bader charge analysis demonstrates that AM adatoms transfer electrons to atoms in their vicinity. The estimated electrons transfer values are 0.87/0.87, 0.84/0.84, 0.8/0.8 e for Li, Na, and K in b-BP(8 AM)@32$H_2$/g-BP(16 AM)@48$H_2$ systems, respectively. It is evident that estimated $E_{ads}$ values correlate with the electron transfer between the AM adatoms and the surrounding atoms. Fig. 3 displays the optimized structures of b-BP(8 AM)@32$H_2$ and g-BP(16 AM)@48$H_2$, whereas the remaining structures of b-BP(8 AM)@$H_2$ and g-BP(16 AM)@$H_2$ are shown in Fig. S6 and Fig. S7. The obtained average H-H bond lengths of adsorbed $H_2$ molecules is in the range of 0.751–0.771 Å (see Table 2). The obtained value is comparable with that of isolated $H_2$ of 0.74 Å.

It should be emphasized that the aforementioned theoretical capacities are evaluated at 0 K. These values exclude the essential thermodynamics contributions of the finite pressure (P) and temperature (T). Here, we explore the thermodynamics analysis of adsorption–desorption properties of b-BP(8 AM)@$H_2$ and g-BP(16 AM)@$H_2$ at the practical conditions. In practice, the P and T values of $H_2$ molecule adsorption are 30 atm and 25 °C, respectively, whereas, the desorption rate takes place at 3 atm and 100 °C [57]. Fig. 4 shows the number of $H_2$ molecules (Nave) adsorbed as a function of P and T. As indicated in Table 3 the obtained capacities of b-BP@8Li, b-BP(8Na), b-BP(8K), g-BP(16Li), g-BP(16Na), and g-BP(16K) are 9.05, 3.27, 0.62, 6.99, 5.23, and 2.30 wt%, respectively. The obtained wt% value is more than the value recently reported for hydrogen storage on defective carbon-based biphenylene monolayer (6.76) [36]. In particular, the $H_2$ molecules storage capacities of b-BP(8Li) and g-BP(16Li) surpass the goal value 5.5 wt% set by the US Department of Energy (DOE) to be achieved by 2025. However, the obtained wt% values for b-BP(8Na/8K)@$H_2$ and g-BP(16Na/16K)@$H_2$ are significantly low. This is due to their weak physisorbed $E_{ads}$ values.

## 4. Conclusions

Inorganic biphenylene materials are becoming a significant family of porous materials for numerous energy-related applications. Particularly, much attention is given to the investigation of $H_2$ storage on these inorganic materials from a theoretical perspective. In the present work, DFT calculations have been performed to study the $H_2$ storage performance of b-BP and g-BP monolayers. Our results reveal that $H_2$ weakly adsorbed on both b-BP and g-BP. However, we found that b-BP(AM) and g-BP(AM) systems improves the $H_2$ molecule $E_{ads}$ value. These b-BP(8 AM) and g-BP(16 AM) systems have been shown to be thermally stable at room temperature. According to bader charge analysis, each AM = Li, Na, K adatoms transferred electrons to the b-BP and g-BP monolayers, making their surfaces suitable to accommodate a significant amount of $H_2$ molecules. We found that the b-BP(8Li), b-BP(8Na), and b-BP(8K) systems can adsorb 32$H_2$ molecules with an average $E_{ads}$ values of −0.18, −0.16, and −0.14 eV/$H_2$. While g-BP(16Li), g-BP(16Na), and g-BP(16K) can accommodate 48$H_2$ molecules with an average $E_{ads}$ values of −0.20,

**Table 2**
Table presents the averaged $E_{ads}$ for several $H_2$ molecules adsorbed on b-BP(AM) and g-BP(AM) systems. $n$ represents the number of $H_2$. $d_{(H-H)}$ is the averaged bond length between H atoms. wt% is the gravimetric density.

| System | $n$ | $E_{ads}$ (eV/$H_2$) | $d_{(H-H)}$ (Å) | $h$ (Å) | wt% |
|---|---|---|---|---|---|
| b-BP(8Li) | 1 | −0.30 | 0.769 | 2.53 | 0.36 |
| | 4 | −0.29 | 0.768 | 2.54 | 1.43 |
| | 8 | −0.27 | 0.765 | 2.84 | 2.81 |
| | 12 | −0.22 | 0.762 | 2.94 | 4.16 |
| | 16 | −0.18 | 0.758 | 3.22 | 5.47 |
| | 32 | −0.18 | 0.759 | 3.45 | 10.38 |
| b-BP(8Na) | 1 | −0.10 | 0.753 | 3.91 | 0.29 |
| | 4 | −0.20 | 0.766 | 3.08 | 1.16 |
| | 8 | −0.19 | 0.764 | 3.10 | 2.30 |
| | 12 | −0.18 | 0.763 | 3.22 | 3.41 |
| | 16 | −0.16 | 0.759 | 3.59 | 4.49 |
| | 32 | −0.16 | 0.758 | 3.63 | 8.60 |
| b-BP(8K) | 1 | −0.03 | 0.751 | 2.95 | 0.25 |
| | 4 | −0.14 | 0.765 | 2.58 | 0.98 |
| | 8 | −0.14 | 0.763 | 2.64 | 1.94 |
| | 12 | −0.14 | 0.761 | 2.66 | 2.89 |
| | 16 | −0.13 | 0.759 | 2.66 | 3.81 |
| | 32 | −0.14 | 0.761 | 2.68 | 7.34 |
| g-BP(16Li) | 1 | −0.30 | 0.767 | 2.58 | 0.18 |
| | 8 | −0.29 | 0.765 | 2.74 | 1.43 |
| | 16 | −0.24 | 0.763 | 2.80 | 2.81 |
| | 24 | −0.20 | 0.762 | 3.02 | 4.16 |
| | 48 | −0.20 | 0.762 | 3.05 | 7.99 |
| g-BP(16Na) | 1 | −0.27 | 0.771 | 2.5 | 0.15 |
| | 8 | −0.20 | 0.767 | 2.78 | 1.16 |
| | 16 | −0.20 | 0.769 | 2.84 | 2.30 |
| | 24 | −0.18 | 0.765 | 3.06 | 3.41 |
| | 48 | −0.17 | 0.765 | 3.08 | 6.59 |
| g-BP(16K) | 1 | −0.22 | 0.770 | 2.60 | 0.12 |
| | 8 | −0.15 | 0.768 | 2.98 | 0.98 |
| | 16 | −0.16 | 0.769 | 2.93 | 1.94 |
| | 24 | −0.13 | 0.765 | 3.40 | 2.89 |
| | 48 | −0.15 | 0.767 | 3.20 | 5.61 |

**Table 3**
The maximum theoretical number of $H_2$ molecules ($N_{theo}$) adsorbed on the host storage b-BP(8 AM) and g-BP(16 AM) systems at T = 0 K. $N_{ads}$ and $N_{des}$ are the number of adsorbed $H_2$ molecules for adsorption (P = 30 atm and T = 25 ℃) and desorption (3 atm and T = 100 ℃) conditions. $N_{prac}$ is the practically usable number of $H_2$ molecules evaluated by $N_{ads} - N_{des}$ . $G_{theo}$ and $G_{prac}$ are the hydrogen theoretical and practical gravimetric capacity (wt%), respectively.

| System | $G_{theo}$ wt% | $N_{theo}$ molecule | $N_{ads}$ molecule | $N_{des}$ molecule | $N_{prac}$ molecule | $G_{prac}$ wt% |
|---|---|---|---|---|---|---|
| b-BP(8Li) | 10.38 | 32 | 30.73 | 3.16 | 27.57 | 9.05 |
| b-BP(8Na) | 8.60 | 32 | 11.88 | 0.19 | 11.69 | 3.27 |
| b-BP(8K) | 7.34 | 32 | 2.65 | 0.04 | 2.61 | 0.62 |
| b-BP(8Li) | 7.99 | 48 | 45.87 | 4.25 | 41.62 | 6.99 |
| g-BP@16Na | 6.59 | 48 | 39.13 | 1.23 | 37.9 | 5.23 |
| g-BP@16K | 5.61 | 48 | 19.43 | 0.29 | 19.14 | 2.30 |

−0.17 and −0.15 eV/$H_2$. The $H_2$ molecules storage capacities of b-BP(8Li)@$H_2$ molecules and g-BP(16Li)@$H_2$ molecules systems attain 9.05 wt% and 6.99 wt% at practical temperature and pressure, respectively. The obtained values exceeding the US Department of Energy's target value of 5.50 wt% by 2025. Based on these findings, metal-functionalized b-BP and g-BP monolayers are promising materials for high-performance $H_2$ storage applications.

## CRediT authorship contribution statement

**Ikram Djebablia:** Data curation, Formal analysis, Investigation, Methodology, Writing – original draft, Conceptualization. **Yusuf Zuntu Abdullahi:** Conceptualization, Data curation, Formal analysis, Investigation, Methodology, Resources, Software, Supervision, Validation, Writing –original draft, Writing –review & editing, Project administration. **Kamel Zanat:** Funding acquisition, Supervision, Writing – original draft. **Fatih Ersan:** Writing –review & editing, Conceptualization, Funding acquisition, Project administration, Software, Supervision, Validation.

## Declaration of competing interest

The authors declare that they have no known competing financial interests or personal relationships that could have appeared to influence the work reported in this paper.

## Acknowledgments

The calculations in this study were performed in the TUBITAK ULAKBIM, High Performance and Grid Computing Center (Tr-Grid e-Infrastructure), and in the Aydin Adnan Menderes University high performance computing facility through the Project Number: FEF-20020. Fatih Ersan thanks to the Science Academy for the BAGEP Award of the Science Academy.

## References

[1] Schlapbach L, Züttel A. Hydrogen-storage materials for mobile applications. Nature 2001;414(6861):353–8.
[2] Niaz S, Manzoor T, Pandith AH. Hydrogen storage: Materials, methods and perspectives. Renew Sustain Energy Rev 2015;50:457–69.
[3] Liu C, Li F, Ma L-P, Cheng H-M. Advanced materials for energy storage. Adv Mater 2010;22(8):E28–62.
[4] Yang J, Sudik A, Wolverton C, Siegel DJ. High capacity hydrogen storage materials: attributes for automotive applications and techniques for materials discovery. Chem Soc Rev 2010;39(2):656–75.
[5] Jena P. Materials for hydrogen storage: past, present, and future. J Phys Chem Lett 2011;2(3):206–11.
[6] Abdullahi YZ, Yoon TL, Mohammad REA. Selective hydrogen adsorption on a buckled carbon nitride sheet: first-principles calculation. Mater Res Express 2018;5(12):125605.
[7] Züttel A. Hydrogen storage methods. Naturwissenschaften 2004;91:157–72.
[8] Chen Z, Kirlikovali KO, Idrees KB, Wasson MC, Farha OK. Porous materials for hydrogen storage. Chem 2022.
[9] Wang H, Liu X, Niu P, Wang S, Shi J, Li L. Porous two-dimensional materials for photocatalytic and electrocatalytic applications. Matter 2020;2(6):1377–413.
[10] Xia Y, Yang Z, Zhu Y. Porous carbon-based materials for hydrogen storage: advancement and challenges. J Mater Chem A 2013;1(33):9365–81.
[11] Abdullahi YZ, Tigli A, Ersan F. Dodecagonal zinc oxide (d-Zn O) monolayer for water desalination and detection of toxic gases. Phys Rev A 2023;19(1):014019.
[12] Abdullahi YZ, Ahmad S, Hui RCY, Ersan F. Porous ZnO-graphenylene sheet for acetylacetone detection. Mater Today Commun 2023;37:107023.
[13] Abdullahi YZ, Ersan F. Theoretical design of porous dodecagonal germanium carbide (d-GeC) monolayer. RSC Adv 2023;13(5):3290–4.
[14] Abdullahi YZ, Ahmad S, Hui RCY. Stability, electronic and optical properties of buckled XO (X=Ge, Cu) graphenylene monolayers: A first-principles study. Solid State Commun 2024;115483.
[15] Chang YHR, Abdullahi YZ, Tuh MH, Yeoh KH. Unveiling the adsorption, activation and reduction of CO2 via inorganic, biphenylene akin Pt-doped ZnMgO2. Inorg Chem Commun 2024;112244.
[16] Chang YHR, Abdullahi YZ, Tuh MH, Lim TL. Ultraviolet enhanced inorganic graphenylene-like ZnMgX2 (X=O, S) for sensitive and reversible detection of toxic formaldehyde at room temperature: A first-principles study. Surf Interfaces 2024;44:103722.
[17] Ahmed S, Ghani A, Muhammad I, Muhammad I, Mehmood A, Ullah N, Hassan A, Wang Y, Tian X, Yakobson B. Enhanced As-COF nanochannels as a high-capacity anode for K and Ca-ion batteries. Phys Chem Chem Phys 2024;26.
[18] Ghani A, Ahmed S, Murtaza A, Muhammad I, Zuo WL, Yang S. Three-dimensional porous tetrakis methane and silane as a high-capacity anode material for monovalent and divalent metal ion batteries. J Phys Chem C 2023;127(34):16802–10.
[19] Muhammad I, Ahmed S, Cao H, Yao Z, Khan D, Mahmood A, Hussain T, Xiong X-G, Ahuja R, Wang Y-G. 3D porous sulfur-graphdiyne with splendid electrocatalytic and energy storage application. Mater Today Chem 2023;34:101756.

[20] Muhammad I, Ahmed S, Yao Z, Khan D, Hussain T, Wang Y-G. First-row transition metal carbide nanosheets as high-performance cathode materials for lithium–sulfur batteries. Nanoscale 2024;16(1):262–72.
[21] Ghani A, Ahmed S, Murtaza A, Muhammad I, ur Rehman W, Zhou C, Zuo WL, Yang S. Bi–C monolayer as a promising 2D anode material for Li, Na, and K-ion batteries. Phys Chem Chem Phys 2023;25(6):4980–6.
[22] Muhammad I, Ahmed S, Cao H, Mahmood A, Wang Y-G. Three-dimensional silicene-based materials: a universal anode for monovalent and divalent ion batteries. J Phys Chem C 2023;127(2):1198–208.
[23] Saeed MH, Ahmed S, Muhammad I, Murtaza I, Ghani A, Ali A, Abdullah R, Khaliq A, et al. Molybdenum carbide nano-sheet as a high capacity anode material for monovalent alkali metal-ion batteries—Theoretical investigation. Phys Lett A 2020;384(27):126688.
[24] Younis U, Muhammad I, Wu W, Ahmed S, Sun Q, Jena P. Assembling Si 2 BN nanoribbons into a 3D porous structure as a universal anode material for both Li-and Na-ion batteries with high performance. Nanoscale 2020;12(37):19367–74.
[25] Nwaji N, Zewdie GM, Gwak J, Kang H, Tufa LT, Choi Y, Goddati M, Shin H, Lee J. Dimeric NiCo single-atom anchored on ultrathin N-doped 2D molybdenum carbide boosted performance in solid-state supercapacitor. J Energy Storage 2024;83:110671.
[26] Kwak IH, Kim JY, Zewdie GM, Yang J, Lee K-S, Yoo SJ, Kwon IS, Park J, Kang HS. Electrocatalytic activation in ReSe2-VSe2 alloy nanosheets to boost water-splitting hydrogen evolution reaction. Adv Mater 2024;2310769.
[27] Fan Q, Yan L, Tripp MW, Krejčí O, Dimosthenous S, Kachel SR, Chen M, Foster AS, Koert U, Liljeroth P, et al. Biphenylene network: A nonbenzenoid carbon allotrope. Science 2021;372(6544):852–6.
[28] Arellano J, Molina L, Rubio A, Alonso J. Density functional study of adsorption of molecular hydrogen on graphene layers. J Chem Phys 2000;112(18):8114–9.
[29] Hashmi A, Farooq MU, Khan I, Son J, Hong J. Ultra-high capacity hydrogen storage in a Li decorated two-dimensional C 2 N layer. J Mater Chem A 2017;5(6):2821–8.
[30] Hussain T, Mortazavi B, Bae H, Rabczuk T, Lee H, Karton A. Enhancement in hydrogen storage capacities of light metal functionalized Boron–Graphdiyne nanosheets. Carbon 2019;147:199–205.
[31] Gao P, Liu Z, Zhang F. Computational evaluation of Li-doped g-C2N monolayer as advanced hydrogen storage media. Int J Hydrogen Energy 2022;47(6):3625–32.
[32] Kassaoui ME, Houmad M, Lakhal M, Benyoussef A, El Kenz A, Loulidi M. Hydrogen storage in lithium, sodium and magnesium-decorated on tetragonal silicon carbide. Int J Hydrog Energy 2021;46(47):24190–201.
[33] Naderizadeh A, Baizaee SM, Kahnouji H. Density functional theory study of reversible hydrogen storage in monolayer beryllium hydride by decoration with boron and lithium. Int J Hydrogen Energy 2023;48(20):7400–18.
[34] Kadioglu Y, Ersan F, Gökoğlu G, Aktürk OÜ, Aktürk E. Adsorption of alkali and alkaline-earth metal atoms on stanene: A first-principles study. Mater Chem Phys 2016;180:326–31.
[35] Alhameedi K, Hussain T, Bae H, Jayatilaka D, Lee H, Karton A. Reversible hydrogen storage properties of defect-engineered C4N nanosheets under ambient conditions. Carbon 2019;152:344–53.
[36] Kaewmaraya T, Thatsami N, Tangpakonsab P, Kinkla R, Kotmool K, Menendez C, Aguey-Zinsou K, Hussain T. Ultrahigh hydrogen storage using metal-decorated defected biphenylene. Appl Surf Sci 2023;629:157391.
[37] Kim J, Kim H, Kim J, Bae H, Singh A, Hussain T, Lee H. Calcium-decorated polygon-graphenes for hydrogen storage. ACS Appl Energy Mater 2023.
[38] Hussain T, Hankel M, Searles DJ. Graphenylene monolayers doped with alkali or alkaline earth metals: promising materials for clean energy storage. J Phys Chem C 2017;121(27):14393–400.
[39] Denis PA, Iribarne F. Hydrogen storage in doped biphenylene based sheets. Comput Theor Chem 2015;1062:30–5.
[40] Mane P, Kaur SP, Chakraborty B. Enhanced reversible hydrogen storage efficiency of zirconium-decorated biphenylene monolayer: a computational study. Energy Storage 2022;4(6):e377.
[41] Mahamiya V, Shukla A, Chakraborty B. Ultrahigh reversible hydrogen storage in K and Ca decorated 4-6-8 biphenylene sheet. Int J Hydrogen Energy 2022;47(99):41833–47.
[42] Jiang M, Xu J, Munroe P, Xie Z-H, Chen Z. Light metal decorated graphene-like Si2BN monolayers as hydrogen storage media: A DFT investigation. Int J Hydrogen Energy 2024;50:865–78.
[43] Yang S, Yin H, Lei G, Lan Z, Wang Z, Xu H, Gu H. A DFT study on the promising hydrogen storage performance of a light metal atom-decorated ZnO monolayer. Int J Hydrogen Energy 2024;50:71–83.
[44] Kaur SP, Hussain T, Kaewmaraya T, Kumar TD. Reversible hydrogen storage tendency of light-metal (Li/Na/K) decorated carbon nitride (C9N4) monolayer. Int J Hydrogen Energy 2023;48(67):26301–13.
[45] Marcos-Viquez AL, Miranda A, Cruz-Irisson M, Pérez LA. Tin carbide monolayers decorated with alkali metal atoms for hydrogen storage. Int J Hydrogen Energy 2022;47(97):41329–35.
[46] Cid BJ, Sosa AN, Miranda Á, Pérez LA, Salazar F, Mtz-Enriquez AI, Cruz-Irisson M. Enhanced reversible hydrogen storage performance of light metal-decorated boron-doped siligene: a DFT study. Int J Hydrogen Energy 2022;47(97):41310–9.
[47] Ploysongsri N, Vchirawongkwin V, Ruangpornvisuti V. Adsorption of hydrogen molecule on alkali metal-decorated hydrogen boride nanotubes: A DFT study. Int J Hydrogen Energy 2021;46(79):39273–83.
[48] Hohenberg P, Kohn W. Inhomogeneous electron gas. Phys Rev 1964;136(3B):B864.
[49] Kresse G, Furthmüller J. Efficient iterative schemes for ab initio total-energy calculations using a plane-wave basis set. Phys Rev B 1996;54(16):11169.
[50] Perdew JP, Burke K, Ernzerhof M. Generalized gradient approximation made simple. Phys Rev Lett 1996;77(18):3865.
[51] Grimme S. Semiempirical GGA-type density functional constructed with a long-range dispersion correction. J. Comput. Chem. 2006;27(15):1787–99.
[52] Monkhorst HJ, Pack JD. Special points for Brillouin-zone integrations. Phys. Rev. B 1976;13(12):5188.
[53] Martyna GJ, Klein ML, Tuckerman M. Nosé–Hoover chains: The canonical ensemble via continuous dynamics. J Chem Phys 1992;97(4):2635–43.
[54] Bader RF. Atoms in molecules. Account Chem Res 1985;18(1):9–15.
[55] Martins NF, Maia AS, Laranjeira JA, Fabris GS, Albuquerque AR, Sambrano JR. Hydrogen storage on the lithium and sodium-decorated inorganic graphenylene. Int J Hydrogen Energy 2024;51:98–107.
[56] Jason JI, Pal Y, Anees P, Lee H, Kaewmaraya T, Hussain T, Panigrahi P. Defects induced metallized boron hydride monolayers as high-performance hydrogen storage architecture. Int J Hydrogen Energy 2024;50:455–63.
[57] Lee H, Choi WI, Ihm J. Combinatorial search for optimal hydrogen-storage nanomaterials based on polymers. Phys Rev Lett 2006;97(5):056104.